MODEL PREDICTIVE MOTION CUEING FOR A HELICOPTER HOVER TASK ON AN 8-DOF SERIAL ROBOT SIMULATOR

Frank M. Drop, Mario Olivari, Stefano Geluardi, Mikhail Katliar, Heinrich H. Bülthoff
{frank.drop, mario.olivari, stefano.geluardi, mikhail.katliar, heinrich.buelthoff}@tuebingen.mpg.de
Max Planck Institute for Biological Cybernetics, Tübingen, Germany

Abstract

Motion cueing for helicopter hover is difficult: small simulators require considerable attenuation, rendering motion cues not useful for stabilization, and large simulators are typically not cost effective. Industrial serial robot-based simulators provide large motion capabilities at a moderate cost, but have two distinct disadvantages. First, they are highly dimensional systems with a non-convex motion space, such that efficient use of the entire space is not trivial. Second, they are typically non-stiff structures with a large mass at the end effector, resulting in oscillatory dynamical properties. We recently developed a novel Model Predictive Motion Cueing Algorithm (MPMCA) that resolves both problems effectively for pre-recorded inertial reference signals. The MPMCA requires an accurate prediction of the future course of the reference inertial signals, which is trivial for pre-recorded maneuvers, but not for real-time human-in-the-loop simulations. In this paper, we present a model-based prediction method, which predicts pilot control inputs and the subsequent helicopter inertial signals during a helicopter hover simulation in real-time. The method is tested in a human-in-the-loop experiment and compared with the Classic Washout Algorithm. The results demonstrate that the MPMCA is a promising new approach to motion cueing.

1. Introduction

The training of helicopter pilots, both novice and advanced, for hover and low-speed maneuvers on a simulator is challenging, but worth pursuing given the obvious safety and cost related advantages over training on an actual helicopter.[1] Simulated training requires accurate motion feedback, because pilots rely heavily on motion at low speeds for stabilization[2,3,4] and improved maneuvering accuracy.[5] Most hover and low-speed maneuvers exceed the motion range offered by conventional Stewart platforms. Thus, a Motion Cueing Algorithm (MCA) is necessary to attenuate the motion by scaling and filtering. The distorted motion might cause the pilot to learn the wrong control strategy, preventing positive transfer of training to the actual rotorcraft. Hence, one typically needs a large, expensive simulator for effective helicopter pilot training.[5]

Simulators based on industrial serial robots provide a potentially large motion space at moderate cost,[6] but have two distinct disadvantages that have not been resolved thus far. First, they are highly dimensional, overactuated systems with a non-convex motion space, such that efficient use of the full motion capabilities is not trivial.[7,8] Second, they are typically non-stiff structures with a large mass at the end effector, resulting in oscillatory motions perceivable by the human,[9] rendering cues that cannot be used for stabilization.

Recently, an MCA based on Model Predictive Control (MPC), was developed for the serial robot-based CyberMotion Simulator (CMS) at the Max Planck Institute for Biological Cybernetics (MPI-BC) that potentially solves both problems.[10] A Model Predictive Motion Cueing Algorithm (MPMCA) calculates a simulator trajectory that optimizes a user-defined cost function over a finite time horizon, based on a *prediction* of the future reference signals, satisfying the limits of the motion system. The reference signals are the inertial signals (specific forces and angular velocities) of the simulated vehicle. The cueing behavior itself is determined by the complexity of the simulator model, correctness of the prediction, and weighting factors in the selected cost function.[11]

A hardware-in-the-loop experiment with pre-recorded low-speed helicopter maneuvers[10] demonstrated that the novel method is able to 1) effectively make use of the *entire* motion space and 2) greatly reduce the effects of oscillatory dynamics.

It is, however, unclear how the method performs in a human-in-the-loop simulation, because the method relies on an accurate prediction of the future reference signal, which is non-trivial given the random nature of helicopter hover maneuvers. That is, in hover, the pilot is predominantly correcting for disturbances caused by random control errors of the pilot *itself*, which are hard to predict.[12]

The objective of this paper is to extend the previous work[10] to an actual human-in-the-loop simulation, which requires a prediction method to be developed. We will describe two prediction methods: a model-free and a model-based approach, which differ considerably in their ease-of-implementation and predictive capabilities. The cueing performance of the methods is compared in computer simulations and the method providing the best objective cueing performance, the model-based approach, is tested in a human-in-the-loop experiment.

The paper is structured as follows. First, the simulated helicopter hover task and the simulation framework is introduced. Then, the MPMCA is briefly introduced, after which we extensively describe the method to reduce the effects of the oscillatory dynamics. The two prediction methods are described in detail, after which we present the results of three experiments. The paper ends with a discussion and conclusions. A supplementary video is provided for additional insight into the method.[13]

2. Simulated helicopter hover

2.1. Simulation overview

In this study, we will consider a simulated helicopter hover task. The pilot is required to hover an identified linear model of the Robinson R44 Raven-II helicopter in front of three hover boards giving visual cues useful for hover. The pilot is seated in the CMS, sees the visual from a projection system and gives control inputs through Pro Flight Trainer PUMA USB controls, see Fig. 1.

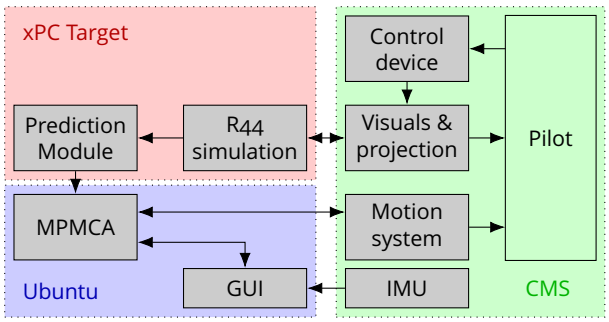

Figure 1: Overview of the simulation framework.

The R44 dynamics run on a MATLAB Simulink xPC target together with the Prediction Module (PM), which calculates the prediction and sends it to the MPMCA, running on a Linux system, which controls the CMS motion system. An Inertial Measurement Unit (IMU) is mounted close to the head position for verification of the method.

2.2. Identified R44 helicopter model

The helicopter model used in this paper was identified from flight test data recorded from a Robinson R44 Raven II helicopter in the hover trim condition.[14] The model is a linear fully coupled 12 degree of freedom (DOF) state-space model valid within the frequency range of 0.3 to 16 rad/s:

$$\dot{\boldsymbol{x}}^{\mathrm{h}} = A\boldsymbol{x}^{\mathrm{h}} + B\boldsymbol{\delta}, \tag{1}$$

$$\boldsymbol{y}^{\mathrm{h}} = C\boldsymbol{x}^{\mathrm{h}} + D\boldsymbol{\delta}, \tag{2}$$

with

$$\boldsymbol{\delta} = [\delta_r, \delta_p, \delta_\psi, \delta_c]^\top, \tag{3}$$

$$\boldsymbol{y}^{\mathrm{h}} = [u, v, w, p, q, r, a_x, a_y, a_z, \phi, \theta]^\top, \tag{4}$$

$$\boldsymbol{x}^{\mathrm{h}} = [u, v, w, p, q, r, \phi, \theta, \beta_{1c}, \beta_{1s}, x_1, x_2, \eta_q, y_1, y_2, \eta_p, \nu, \beta_0, \dot{\beta}_0, \eta_{C_t}]^\top, \tag{5}$$

in which $[\delta_r, \delta_p, \delta_\psi, \delta_c]$ are cyclic roll, cyclic pitch, pedals, and collective pitch control inputs, $[u, v, w]$ are the linear velocities, $[p, q, r]$ are the angular velocities, $[a_x, a_y, a_z]$ are the linear accelerations, $[\phi, \theta]$ are the roll and pitch angles, $[\beta_{1c}, \beta_{1s}]$ are the rotor-flap/body coupling dynamics, $[x_1, x_2, \eta_q, y_1, y_2, \eta_p]$ are the lead-lag dynamics and $[\nu, \beta_0, \dot{\beta}_0, \eta_{C_t}]$ are the coning-inflow dynamics.[15] Matrix values are given in Ref. 14.

The inertial signals, to be followed by the MPMCA, consist of the specific forces and angular velocities as measured at the pilot head reference position. The specific forces are the sum of the accelerations of the helicopter and the contribution of gravity, resolved into the head reference frame:

$$\boldsymbol{f} = -\boldsymbol{a} + R_{\mathrm{W}}^{\mathrm{H}}\mathbf{g}, \tag{6}$$

with $\boldsymbol{a} = [a_x, a_y, a_z]^\top$, $\mathbf{g} = [0, 0, g]^\top$ the gravitational specific force vector, and $R_{\mathrm{W}}^{\mathrm{H}}$ the world to head transformation matrix. The angular velocities are outputs of the model: $\boldsymbol{\omega} = [\omega_x, \omega_y, \omega_z] = [p, q, r]$.

3. Model predictive motion cueing

Recently, an MPMCA for real-time control of the CMS was developed.[10] The goal of the controller is

to accurately reproduce the reference inertial signal $\hat{\boldsymbol{y}} = [\hat{f}_x, \hat{f}_y, \hat{f}_z, \hat{\omega}_x, \hat{\omega}_y, \hat{\omega}_z]^\top$. At every control interval, the MPMCA is given a *prediction* of the future T_p seconds of the reference signal $\hat{\boldsymbol{y}}^{\mathrm{p}}$ consisting of N equally spaced samples. The MPMCA computes a sequence of N control inputs $U = [\boldsymbol{u}_0, \boldsymbol{u}_1, \ldots, \boldsymbol{u}_{N-1}]$ which are the solution of the following optimization problem:

$$
\begin{aligned}
\min_{X,U} \quad & J(X,U) \\
\text{s.t.} \quad & \boldsymbol{x}_0 = \tilde{\boldsymbol{x}}_0, \\
& \boldsymbol{x}_{k+1} = F(\boldsymbol{x}_k, \boldsymbol{u}_k),\ k = 0 \ldots N-1, \\
& \underline{\boldsymbol{x}}_k \le \boldsymbol{x}_k \le \overline{\boldsymbol{x}}_k, \qquad k = 1 \ldots N, \\
& \underline{\boldsymbol{u}} \le \boldsymbol{u}_k \le \overline{\boldsymbol{u}}, \qquad k = 0 \ldots N-1,
\end{aligned} \tag{7}
$$

in which the objective function J is defined as:

$$
\begin{aligned}
J(X,U) = \frac{1}{N} \sum_{k=0}^{N-1} \Big(& \|y(\boldsymbol{x}_k, \boldsymbol{u}_k) - \hat{\boldsymbol{y}}_k\|^2_{W_{\boldsymbol{y}}} \\
& + \|\boldsymbol{x}_k - \hat{\boldsymbol{x}}\|^2_{W_{\boldsymbol{x}}} + \|\boldsymbol{u}_k\|^2_{W_{\boldsymbol{u}}} \Big) + \|\boldsymbol{x}_N - \hat{\boldsymbol{x}}\|^2_{W_{\boldsymbol{x}_N}} .
\end{aligned} \tag{8}
$$

and $\boldsymbol{x}_k$ is the simulator state at prediction time step k, $X = [\boldsymbol{x}_0, \boldsymbol{x}_1, \ldots, \boldsymbol{x}_N]^\top$, $\hat{\boldsymbol{x}}$ is a selected neutral state, $\underline{\boldsymbol{x}}$, $\overline{\boldsymbol{x}}$, $\underline{\boldsymbol{u}}$, and $\overline{\boldsymbol{u}}$ are the lower and upper bounds of the state and control input, and F the function defining the discrete-type dynamics of the simulator.

The output function y defines the mapping from the simulator state and control input to the resulting *expected* inertial signal $\boldsymbol{y}^{\mathrm{e}}$, which might be different from the *actual* inertial signal $\boldsymbol{y}^{\mathrm{m}}$ measured by the IMU at the pilot head location.

The optimal solution to (7) constitutes a trade-off between the output error term weighted by the symmetric positive-definite weighting matrix $W_{\boldsymbol{y}}$, and the washout, input, and terminal cost terms weighted by $W_{\boldsymbol{x}}$, $W_{\boldsymbol{u}}$, and $W_{\boldsymbol{x}_N}$, respectively.[11] The selected numerical values of the weighting matrices will determine 1) the importance of each output signal with respect to other outputs, and 2) the relative importance of tracking the reference output or maintaining a small distance to the neutral state. The first is determined only by values in the $W_{\boldsymbol{y}}$ matrix, while the latter is determined by values in both the $W_{\boldsymbol{y}}$ and $W_{\boldsymbol{x}}$ matrices.

In this study, the prediction horizon T_p was 4.9 s, sampled at 12ms, such that $N = 409$. See Table 1 for weighting matrix and washout position values.

4. Structural oscillations

The simulator, consisting of a long and slender robot arm to which the heavy cabin is attached, behaves as a badly damped harmonic oscillator causing unintended accelerations. See Fig. 2 for a typical response of the simulator to a step input commanded by the MPMCA. The *expected* lateral specific force f_y^{e} follows the reference doublet input $\hat{f}_y$ accurately, but the *measured* lateral specific force f_y^{m} is very different from f_y^{e}. The high frequency oscillations have amplitudes far exceeding the amplitude of the doublet itself and take more than 4 s to dampen out. To mitigate these oscillations,[16] we identify a model of the oscillatory dynamics and include it in the simulator model, such that the MPMCA avoids exciting these dynamics.

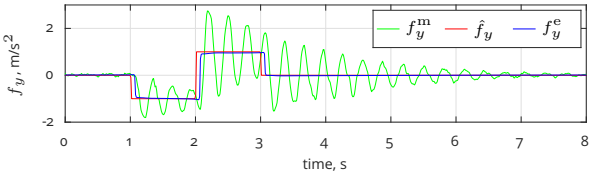

Figure 2: Typically observed oscillatory accelerations.

4.1. Measuring and modeling oscillations

The oscillatory dynamic were measured by providing a sum-of-sines forcing function as $\hat{\boldsymbol{f}}$ to the MPMCA. Measurements were performed separately for the longitudinal, lateral, and vertical specific forces. The sum-of-sine signal consisted of 15 sines with frequencies ω_d between 0.3 and 45 rad/s, with randomly chosen phase shifts. An estimate of the oscillatory dynamics at frequencies ω_d was obtained from the Best Linear Approximation (BLA) method:[17]

$$
\tilde{H}_{\mathrm{o}}(\omega) = \frac{S_{\hat{\boldsymbol{f}},\boldsymbol{f}^{\mathrm{m}}}(\omega)}{S_{\hat{\boldsymbol{f}},\boldsymbol{f}^{\mathrm{e}}}(\omega)}, \quad \omega \in \{\omega_d\}, \tag{9}
$$

Table 1: Washout position and weighting matrix values.

$W_{\boldsymbol{y}}$	$\mathrm{diag}([1, 1, 0.5, 10, 10, 10])^2$
$W_{\boldsymbol{u}}$	$\mathrm{diag}([0.2, 0.5, 0.5, 0.5, 0.5, 0.5, 0.5, 0.2])^2$
$W_{\boldsymbol{x}}$	$\mathrm{diag}([0.012, 0, 0.02, 0.02, 0.02, 0.02, 0.02, 0.02, \mathbf{0}^{1\times 8}])^2$
$W_{\boldsymbol{x}_N}$	$\mathrm{diag}([0.012, 0, 0.02, 0.02, 0.02, 0.02, 0.02, 0.02, \mathbf{0}^{1\times 8}])^2$
$\hat{\boldsymbol{x}}$	$[4.45, -1.15, -1.44, 1.42, 1.51, 0.30, -1.51, 1.55, \mathbf{0}^{1\times 8}]$

where $S_{\hat{\boldsymbol{f}},\boldsymbol{f}^{\mathrm{m}}}$, $S_{\hat{\boldsymbol{f}},\boldsymbol{f}^{\mathrm{e}}}$ are the estimated cross-spectral densities between each component of $\hat{\boldsymbol{f}}$, $\boldsymbol{f}^{\mathrm{e}}$, and $\boldsymbol{f}^{\mathrm{m}}$, and subscript o denoting the Oscillation Model (OM). A linear transfer function model H_{o} with two zeros and two poles was then fit to estimate $\tilde{H}_{\mathrm{o}}$:

$$H_{\mathrm{o}}(s,\ \mathbf{p}) = \frac{a_2 s^2 + a_1 s + 1}{b_2 s^2 + b_1 s + 1}, \tag{10}$$

with $\mathbf{p} = [a_1, a_2, b_1, b_2]$, by minimizing:

$$\arg\min_{\mathbf{p}} \sum_{\omega \in \{\omega_d\}} \left\| \log\left(\frac{H_{\mathrm{o}}(j\omega,\ \mathbf{p})}{\tilde{H}_{\mathrm{o}}(\omega)} \right) \right\|^2. \tag{11}$$

Fig. 3 shows $\tilde{H}_{\mathrm{o}}$ and H_{o} for the lateral axis; a good fit in the frequency domain was obtained, suggesting that the order of H_{o} was chosen correctly.

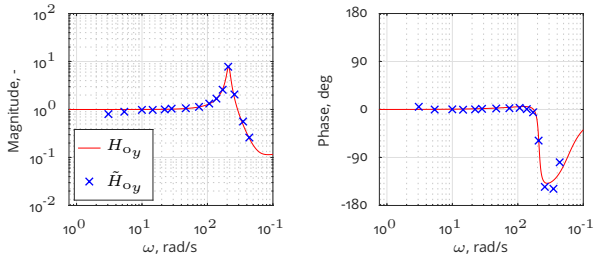

Figure 3: Estimated dynamics for lateral structural oscillations.

Fig. 4 shows the simulated response of H_{o_y} to f_y^{e} compared to f_y^{m}, for a doublet reference on $\hat{f}_y$. The fitted model reproduces f_y^{m} reasonably well, although the measured oscillations persist for longer than the simulated oscillations. Attempts to capture this behavior by further lowering the damping ratio in the model lead to considerably worse fits at the doublet onsets. It seems that the oscillatory behavior also involves considerable couplings in other directions of motion. Accounting for these effects is planned for future work.

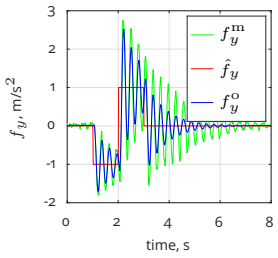

Figure 4: Simulated response f_y^{o} of H_{o_y} to doublet reference compared to the measured response.

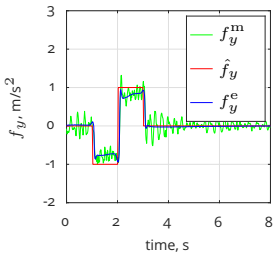

Figure 5: Measured response to doublet when including H_{o} in the simulator model.

The transfer functions obtained for all axes are listed in Tab. 2. They were rewritten into second-order model form, to highlight damping ratios ζ_n and natural frequencies ω_n:

$$H_{\mathrm{o}} = \frac{\omega_n^2}{\bar{\omega}_n^2} \cdot \frac{s^2 + 2\bar{\omega}_n\bar{\zeta}_n s + \bar{\omega}_n^2}{s^2 + 2\omega_n\zeta_n s + \omega_n^2} = \frac{[\bar{\zeta}_n,\ \bar{\omega}_n]}{[\zeta_n,\ \omega_n]}. \tag{12}$$

Table 2: OM coefficients, natural frequencies and damping ratios. Coefficients a_1, a_2, b_1, and b_2 were multiplied by 10^3.

Axis	a_1	a_2	b_1	b_2	H_{o}
f_x	0.8	2.2	1.7	10.6	$\begin{bmatrix} 0.04,\ 36.4 \\ 0.13,\ 24.2 \\ 0.46,\ 58.6 \end{bmatrix}$
f_y	0.3	15.8	2.2	5.6	$\begin{bmatrix} 0.06,\ 21.1 \\ 0.41,\ 46.5 \end{bmatrix}$
f_z	0.5	17.5	1.4	7.7	$\begin{bmatrix} 0.10,\ 27.0 \end{bmatrix}$

4.2. Mitigating oscillations

The identified OMs were included in the model of the serial robot dynamics, by augmenting the discrete-time dynamics and output functions, F and y, with a discretization of H_{o}:

$$F_{\mathrm{o}}(\boldsymbol{x}_k^{\mathrm{a}}, \boldsymbol{u}_k^{\mathrm{a}}) = \begin{bmatrix} A_{\mathrm{a}} & 0 \\ 0 & A_{\mathrm{o}} \end{bmatrix} \boldsymbol{x}_k^{\mathrm{a}} + \begin{bmatrix} B_{\mathrm{a}} & 0 \\ 0 & B_{\mathrm{o}} \end{bmatrix} \boldsymbol{u}_k^{\mathrm{a}}, \tag{13}$$

$$y_{\mathrm{o}}(\boldsymbol{x}_k^{\mathrm{a}}, \boldsymbol{u}_k) = \begin{bmatrix} 0 & C_{\mathrm{o}} \\ 0 & 0 \end{bmatrix} \boldsymbol{x}_k^{\mathrm{a}} + \begin{bmatrix} D_{\mathrm{o}} & 0 \\ 0 & I \end{bmatrix} \boldsymbol{u}_k^{\mathrm{a}}, \tag{14}$$

with

$$\boldsymbol{u}_k^{\mathrm{a}} = \begin{bmatrix} \boldsymbol{f}^{\mathrm{e}}(\boldsymbol{x}_k, \boldsymbol{u}_k) \\ \boldsymbol{\omega}^{\mathrm{e}}(\boldsymbol{x}_k) \end{bmatrix}, \tag{15}$$

where A_{o}, B_{o}, C_{o}, D_{o} are the discrete-time state-space matrices corresponding to H_{o}, and A_{a}, B_{a} the discrete-time state-space matrices of the robot. $\boldsymbol{\omega}^{\mathrm{e}}$ is not considerably affected by oscillations, and is thus directly fed through in y_{o}.

Fig. 5 shows a measured response of the real system to a doublet reference signal, if the OM is included in the MPMCA. The structural oscillations are clearly reduced. Tab. 3 quantifies the improvements by listing the Root Mean Square (RMS) errors between $\boldsymbol{f}^{\mathrm{e}}$ and $\boldsymbol{f}^{\mathrm{m}}$, with and without OM, for the reference doublet of Fig. 4. The improvement is especially large in the lateral DOF, where the RMS error was reduced by a factor of 4.

5. Prediction methods

The MPMCA requires an accurate *prediction* $\hat{\boldsymbol{y}}^{\mathrm{p}}$ of the future T_p s of the reference output $\hat{\boldsymbol{y}}$. The requirements on the accuracy of the prediction for

Table 3: RMS errors between $\boldsymbol{f}^{\mathrm{e}}$ and $\boldsymbol{f}^{\mathrm{m}}$.

Axis	RMS, m/s^2	
	without OM	with OM
x	0.15	0.11
y	0.45	0.11
z	0.13	0.12

acceptable cueing are unknown. Predictions can be generated with model-free prediction methods (FPMs), model-based prediction methods (MPMs), and methods that combine both approaches. First, we discuss the potential (dis)advantages of each method, and then present the two methods considered for further analysis in this paper.

5.1. Background

5.1.1. Model-free prediction methods

FPMs calculate $\hat{\boldsymbol{y}}^{\mathrm{p}}$ from current or past values of $\hat{\boldsymbol{y}}$. Potential methods range from simple N-th order polynomial extrapolation to more complex statistical signal forecasting methods. FPMs might, arguably, be able to predict the near future reasonably well, but might perform worse further into the future. To prevent clearly wrong far-future predictions from affecting cueing behavior too much, it might be beneficial to smoothly morph the extrapolated signals into a predetermined value. One might chose to let signals decay to zero, assuming that transients are short, after which the vehicle returns to a steady-state condition where inertial signals are generally small or zero.

FPMs have certain potential advantages: 1) they are easy to implement, as they work independently from other elements in the simulation, 2) they typically require small computational effort, and 3) the influence of each parameter in the method on the predicted output is straightforwardly examined.

We foresee the following potential disadvantages. First, they will not be able to predict strong transients, such as the onset of turns or strong wind gusts. Such transients are, however, exactly the problematic areas for traditional MCAs we wish to improve. Second, even though the effect of a parameter in the method on the predicted signal is easily examined, its effect on the cueing behavior and feel is not. Thus, these parameters need to be 'tuned' in human-in-the-loop experiments: a tedious and time-consuming process.

5.1.2. Model-based prediction methods

MPMs attempt to predict the future by simulating a model of the control task at hand. The model may contain (simplified) models of the vehicle and human control behavior. Simple methods may assume the current human control inputs to remain constant and simulate the resulting vehicle response. More complex methods might involve a simplified model of human control dynamics, or may even utilize non-trivial inputs, such as physiological measurements, to predict human decision taking when the human is free to decide which path to follow in the virtual world.

MPMs have certain potential advantages. First, the utilization of an accurate vehicle dynamics model should result in 'congruent' inertial signals. For example, a constant cyclic roll input will, depending on the current state of the helicopter, result in different combinations of roll rate and lateral acceleration: something a model-free method cannot predict. Second, the method can also predict transients, such as turn onsets, if it is aware of the expected future path of the vehicle. Third, assuming that cueing always improves if more accurate predictions are provided, ultimately with the best cueing for a perfect prediction, then one can avoid a considerable amount of tedious 'tuning' while developing the prediction method. That is, the predictive capabilities can be objectively validated with pre-recorded data, and thus continuous testing on human-in-the-loop simulations is not necessary.

Obviously, MPMs also have disadvantages. First, if the vehicle dynamics are unstable, it is not possible to construct a prediction simulation without a stabilizing controller. The stabilizing controller *should* then resemble human control behavior, which might be difficult to achieve. Second, if the human decides to do something very different from what is predicted, cueing might be unacceptably bad and invoke motion sickness.

5.2. Implemented prediction methods

5.2.1. Exponential decay prediction

In this paper, we limit our scope to an easy-to-compute FPM with only one parameter needing manual selection. The Exponential Decay Prediction (EDP) method predicts the current value of each individual inertial channel to decay to zero following the exponential function:

$$\hat{\boldsymbol{y}}^{\mathrm{p}}(t_p;t) = \hat{\boldsymbol{y}}(t)e^{-\alpha t_p}, \tag{16}$$

with t_p the prediction horizon time parameter running from 0 to T_p, and α determining the exponential decay rate, which needs to be chosen by the user. Fig 6 plots (16) for different values of α. Note that for $\alpha = 0$ the method reduces to the 'constant' prediction method, i.e., the signal is predicted to remain constant until T_p. The exponential

function was selected, because it contains only one parameter, decays asymptotically to zero without overshoot, and is continuous in all its derivatives.

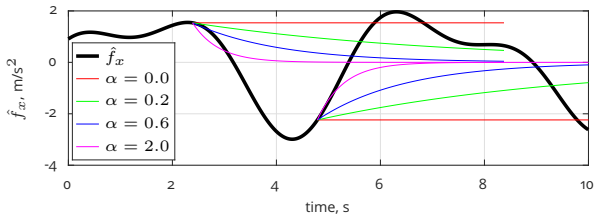

Figure 6: Exponential function (16) for different α.

5.2.2. Pilot Model Prediction

The model-based prediction method considered in this paper consists of a "prediction simulation" running inside the main simulation, see Fig. 7. It is referred to here as the Pilot Model Prediction (PMP) method. The main simulation runs at 6 ms intervals in real-time, and the prediction simulation is executed at every control interval j of the MPMCA, from time-step $k = j$ to $j + N$, to calculate $\hat{\boldsymbol{y}}^{\mathrm{p}}$. In the prediction simulation, a model of the pilot substitutes for the human pilot in the main simulation.

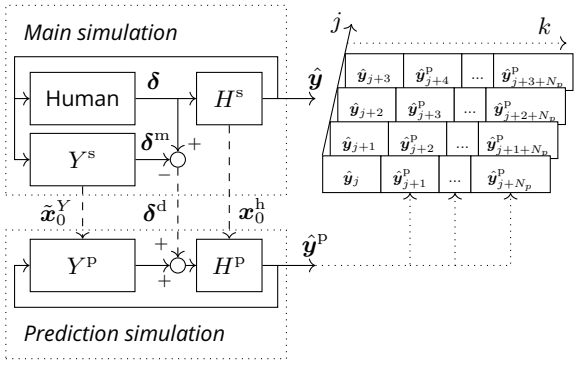

Figure 7: Schematic overview of the Pilot Model Prediction method, with the helicopter dynamics denoted H, and the pilot dynamics denoted Y.

In Fig. 7, the pilot model Y appears twice: once in the main simulation Y^{s} and once in the prediction simulation Y^{p}. The pilot model in the main simulation receives the output of H^{s} to obtain estimate $\tilde{\boldsymbol{x}}_0^Y$ of the state of the human pilot. This state estimate is necessary to initialize the prediction simulation. The difference $\boldsymbol{\delta}^{\mathrm{d}}$ between the human control input $\boldsymbol{\delta}$ and the model control input $\boldsymbol{\delta}^{\mathrm{m}}$ is added to the control output of Y^{p} as a constant disturbance signal, to ensure continuity between $\hat{\boldsymbol{y}}$ and $\hat{\boldsymbol{y}}^{\mathrm{p}}_{j+1}$.

The pilot model consists of four independent, linear control loops responding to helicopter states and outputs perceivable to the human. The vertical position and yaw heading are controlled by a single loop. The lateral and longitudinal degrees of freedom are controlled by a inner loop on roll and pitch, respectively, and an outer loop on translational *velocity*. It was found that f_x^{p}, f_y^{p}, ω_x^{p} and ω_y^{p} were more accurate, if the pilot was assumed to drive the velocity to zero, rather than the position.

The limited field of view in the simulator makes it hard to see the intended hover spot, such that effective position feedback is impossible. Pilots were found to slowly drift to a position away from the initial position, and then attempt to maintain the new position, as if it was the intended position.

For some helicopter dynamics, models of pilot control dynamics were identified from human-in-the-loop experimental data.[12] For others, we assumed that the Crossover Model[18] would hold and designed the pilot model such that the combined pilot-helicopter dynamics approximate a single integrator and a time delay around the crossover frequency. The selection of the proper pilot model dynamics was guided by deriving the on-axis transfer functions from the helicopter state space model. The transfer functions were obtained by selecting the on-axis terms from the state-space matrices.[19] For example, the on-axis dynamics from δ_r to lateral outputs involves only the states $[v, a_y, p, \phi, \beta_{1s}, y_1, y_2, \eta_p]$.

Vertical position controller The objective of the vertical position controller is to hold a constant position by rejecting disturbances. We expect the pilot to use a purely feedback control strategy, because the disturbances are unpredictable.[20] Fig. 8 depicts the feedback organization adopted by the pilot.

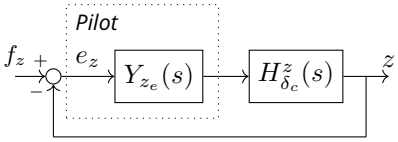

Figure 8: Pilot model block diagram for the vertical position controller (yaw controller has identical structure). In hover, the target signals f_z and f_ψ are equal to zero.

The collective to vertical position dynamics are:

$$H^z_{\delta_c}(s) = \frac{z(s)}{\delta_c(s)} = \frac{0.75(s+6.7)}{s(s+0.34)(s+9.5)}. \quad (17)$$

The zero at 6.7 rad/s and the pole at 9.5 rad/s are unlikely to influence the adopted pilot feedback dynamics, because they are close to each other and considerably above the crossover frequency. Thus, the feedback dynamics are assumed to take the same form as those seen[18] in pure second-order systems of the form $K/s(s + \omega)$, consisting of a

Table 4: Pilot model parameter values.

Param.	Value	Unit	Param.	Value	Unit
K_{v_e}	-0.008	-	K_{ϕ_e}	2.5	-
K_{v_e}	0.008	-	K_{θ_e}	3.3	-
K_{z_e}	1.67	-	K_{ψ_e}	3.3	-
K_{ϕ_t}	1.0	-	K_{θ_t}	1.0	-
$T_{u_e^1}$	4	s	$T_{v_e^1}$	4	s
$T_{u_e^2}$	0.15	s	$T_{v_e^2}$	0.3	s
$T_{\phi_e^1}$	0.55	s	$T_{\theta_e^1}$	1.35	s
$T_{\phi_e^2}$	5.0	s	$T_{\theta_e^2}$	5.0	s
T_{z_e}	3.0	s	T_{ψ_e}	0.9	s
T_{ϕ_t}	0.2	s	T_{θ_t}	0.2	s
τ_{ϕ_e}	0.25	s	τ_{θ_e}	0.25	s
τ_{ψ_e}	0.25	s	τ_{z_e}	0.25	s
τ_{ϕ_t}	0.1	s	τ_{θ_t}	0.1	s
ω_{nms}	12.5	rad/s	ζ_{nms}	0.3	-

gain, a lead, a time delay and neuromuscular system (NMS) dynamics:

$$Y_{z_e}(s) = K_{z_e}(T_{z_e}s + 1)e^{-\tau_{z_e}s}Y_{nms}(s). \quad (18)$$

See Table 4 for parameter values. Fig. 9 shows Bode plots of the helicopter and pilot dynamics, and the open loop transfer function from which the crossover frequency and phase margin can be derived. The selected parameter values result in a crossover frequency of 2.8 rad/s, which is relatively high compared to values measured in experiments without motion feedback.[21] Here, pilots can generate lead from the perceived physical motion cues, thereby effectively reducing τ_{z_e}, allowing for a higher gain, increasing the crossover frequency.[2,3]

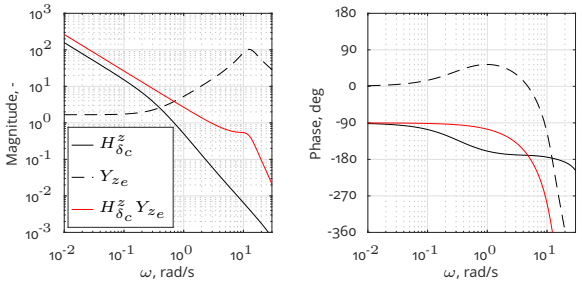

(a) Magnitude. (b) Phase.

Figure 9: Bode plots of the helicopter and pilot transfer functions for the vertical position control loop.

The NMS dynamics model represents the combined dynamics of the arms or legs of the pilot and the control device.[22] The NMS dynamics are modeled as an underdamped mass-spring-damper system, with identical parametrization for all DOFs:

$$Y_{nms}(s) = \frac{\omega_{nms}^2}{s^2 + 2\zeta_{nms}\omega_{nms}s + \omega_{nms}^2}. \quad (19)$$

Yaw controller The helicopter pedal to yaw position transfer function is given as:

$$H^{\psi}_{\delta_{\psi}}(s) = \frac{0.31}{s(s + 1.1)}. \quad (20)$$

The pilot will adopt the same control organization as depicted in Fig. 8 for the vertical position loop. The pilot feedback dynamics in response to this second-order system will consist of a gain, a lead, and a time delay, and NMS dynamics:

$$Y_{\psi_e}(s) = K_{\psi_e}(T_{\psi_e}s + 1)e^{-\tau_{\psi_e}s}Y_{nms}(s). \quad (21)$$

The selected gain results in a crossover frequency of 0.92 rad/s, see Fig. 10, which is lower than typical crossover values, which are usually measured for joystick control devices and not for pedals operated by the feet.

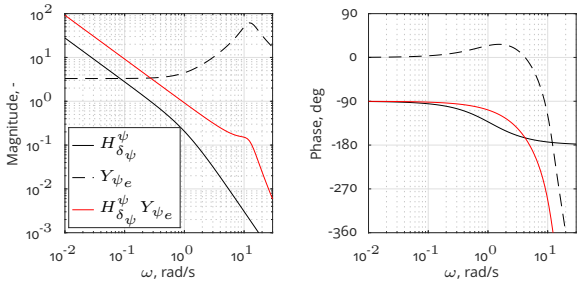

(a) Magnitude. (b) Phase.

Figure 10: Bode plots of helicopter and pilot transfer functions for the yaw position control loop.

Longitudinal and lateral controllers The pitch-longitudinal and roll-lateral controllers have identical form, but different parameterizations. The pitch-longitudinal controller consists of an outer loop rejecting disturbances in the forward velocity u, by generating the pitch target θ_t which is tracked by the inner loop around θ, see Fig. 11.

The outer loop controller dynamics should equalize the combined dynamics of 1) the inner loop pitch controller, 2) the helicopter pitch dynamics, and 3) the helicopter pitch to forward velocity dynamics. Here, we assume the combined dynamics of the first two elements to be approximately equal to a unity gain and a considerable lag. The helicopter pitch to forward velocity dynamics are approximately equal to:

$$H^{u}_{\theta}(s) = \frac{0.72(s - 3.7)(s + 3.7)}{(s + 0.25)}. \quad (22)$$

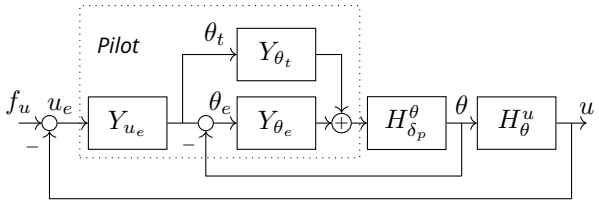

Figure 11: Pilot model block diagram for longitudinal velocity and pitch attitude.

To the best of the authors' knowledge, no studies investigated the feedback structure adopted by human pilots when confronted with such system dynamics. Therefore, we assume outer loop feedback dynamics that stabilize H^u_θ by pole-zero cancellation, such that the combined open loop transfer function approximates an integrator around the crossover frequency.[18] The outer loop feedback controller dynamics are given as:

$$Y_{v_e}(s) = K_{v_e}\frac{(T_{v_e^1}s+1)}{(T_{v_e^2}s+1)^2}, \tag{23}$$

with $T_{v_e^1}$ cancelling the pole at 0.25 rad/s, and $T_{v_e^2}$ the zeros at 3.7 rad/s, see Table 4.

The pitch controller tracks the pitch target of the outer loop controller with a combined feedforward and feedback control strategy.[21,23] The helicopter cyclic pitch to pitch angle transfer function is:

$$H^\theta_{\delta_p}(s) = \frac{3.4(s+0.25)}{(s+38)(s-0.5)(s^2+1.1s+0.64)}. \tag{24}$$

Experimental studies investigating human feedforward or feedback responses did not consider identical dynamics. A set of similar system dynamics was considered in Ref. 24, whose results give reasons to assume that the feedback dynamics will consist a gain, *a double lead*, a time delay and NMS dynamics, omitting argument s for aesthetic reasons:

$$Y_{\theta_e} = K_{\theta_e}\frac{(T_{\theta_e^1}s+1)(T_{\theta_e^2}s+1)}{s}e^{-\tau_{\theta_e}s}Y_{nms}, \tag{25}$$

with $T_{\theta_e^1}$ and $T_{\theta_e^2}$ placed close to the majority of the poles and zeros of (24) to obtain single integrator open loop dynamics around crossover.

The hover performance of the pilot model without a feedforward element was found to be considerably worse than actual human hover performance. Therefore, a feedforward path consisting of a gain, inverse system dynamics, and a time delay,[23] was included, which improved performance:

$$Y_{\theta_t}(s) = K_{\theta_t}\frac{1}{H^\theta_{\delta_p}}\frac{1}{(T_{\theta_t}s+1)^2}e^{-\tau_{\theta_t}s}. \tag{26}$$

Bode plots of all inner and outer loop pilot and helicopter transfer functions are shown in Fig. 12 for the longitudinal and pitch controllers.

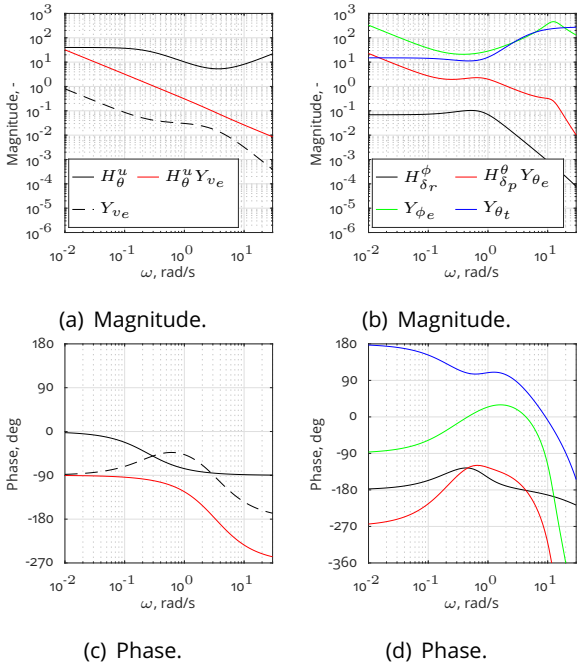

(a) Magnitude. (b) Magnitude.

(c) Phase. (d) Phase.

Figure 12: Bode plots of helicopter and pilot transfer functions for the outer and inner control loops on longitudinal velocity and pitch angle. Bode plots for lateral velocity and roll angle are similar.

6. MPMCA Cueing Example

So far, this paper presented many concepts novel to motion cueing. Section 3 introduced the Model Predictive Controller, which calculates the optimal simulator trajectory based on a prediction of the future inertial reference signal. Section 4 presented our efforts to mitigate undesired accelerations due to the oscillatory dynamics of the CMS. Then, Section 5 presented two methods for calculating the prediction of future inertial reference signals. Before continuing the paper, we present data collected during a human-in-the-loop simulation, to provide insight into the cueing obtained with the MPMCA if the PMP method is used for prediction and the OM is included in the controller. A supplementary video is provided for additional insight into the method.[13]

6.1. Prediction

Fig. 13 compares the predicted inertial signals f_x^{p} and ω_x^{p} to the actual reference signals $\hat{f}_x$ and $\hat{\omega}_x$, plotted starting from the point in time when the predictions were made. Predicted longitudinal specific forces, f_x^{p}, see Fig. 13(a), resemble $\hat{f}_x$ reason-

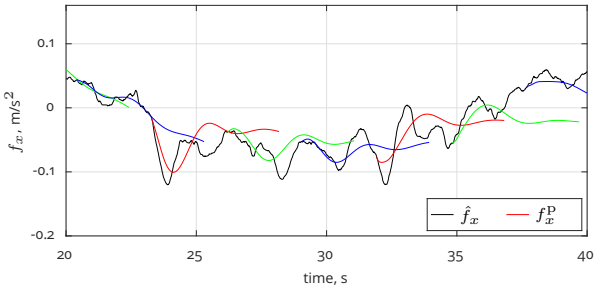

(a) Longitudinal specific force.

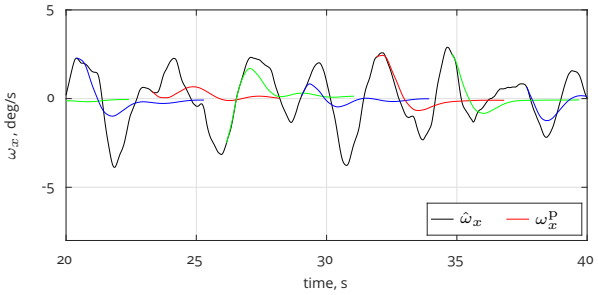

(b) Roll angular velocity.

Figure 13: Example of predicted inertial signals by the PMP during a simulation. All colored lines resemble predictions.

ably well during the first 2 s of the horizon, but then start to deviate, in approximately 50% of the cases. Other predictions deviate directly from the start. Note that the predicted accelerations converge to a nonzero value, which is caused by $\boldsymbol{\delta}^{\mathrm{d}}$, see Fig. 7. In most cases, this improves the prediction, as $\hat{f}_x$ returns to zero very slowly.

Predicted roll rates, ω_x^{p}, see Fig. 13(a), are often correct in direction, magnitude and phase, especially during the first 2 s of the horizon. The obtained results suggest that the inner loop controllers resemble actual human behavior quite well, while the outer loop controllers need improvement.

6.2. Cueing

Fig. 14 and 15 show the reference $\hat{\boldsymbol{y}}$, expected $\boldsymbol{y}^{\mathrm{e}}$, and measured $\boldsymbol{y}^{\mathrm{m}}$ inertial signals for each component as produced by the MPMCA. The expected output of the Classic Washout Algorithm (CWA) $\boldsymbol{y}^{\mathrm{cwa}}$, see Appendix A, that would result from applying the same reference output, is shown for comparison.

6.2.1. Specific forces

The plotted measured specific forces $\boldsymbol{f}^{\mathrm{m}}$ were low-pass filtered with a second-order Butterworth filter with a cutoff frequency of 2.5 Hz. Above 2.5 Hz, the effects of the oscillatory dynamics of the CMS are still clearly visible and would make it hard to see the low-frequent differences that exist between $\boldsymbol{f}^{\mathrm{e}}$ and $\boldsymbol{f}^{\mathrm{m}}$, see Fig. 14. These small differences are caused by 1) the IMU placement: it cannot be exactly in the head-reference point, it is approximately 20 cm behind and to the right of the head, 2) possible discrepancies in the kinematic model, 3) other electromechanical effects in the system that might cause undesired tilting of the cabin, such as play.

The expected specific forces of the MPMCA follow the reference in the longitudinal and lateral DOFs quite well, but not so good in the vertical DOF. That is, most fluctuations in $\hat{f}_x$ and $\hat{f}_y$ are reproduced in f_x^{e} and f_y^{e} by forces in the same direction, with similar magnitude, and generally in-phase; differences are often low-frequent offsets. Larger fluctuations in $\hat{f}_z$ are attenuated considerably, however, and negatively affect the cueing of $\hat{f}_x$ and $\hat{f}_y$, as seen between 20 and 31 s and again between 42 and 52 seconds. Here, the MPMCA cannot reproduce all three specific forces simultaneously, and sacrifices some dexterity in the horizontal plane, resulting in some false cues in f_x^{e} and f_y^{e}, in return for more vertical motion capabilities. If desired, this tendency can be reduced by increasing the weights on f_x and f_y, or reducing the weight on f_y in $W_{\boldsymbol{y}}$.

Fig. 16(a) shows a detail of Fig. 14(a). Observe that before 32 s, the oscillations in f_x^{m} are much larger than after, even though f_x^{e} contains similar fluctuations. The OM is, apparently, able to cancel out certain vibrations, but not all. Possibly, the OM should also consider potential couplings between excitations in different directions.

6.2.2. Angular velocities

The reproduction of the angular velocities by the MPMCA is very good in all DOFs, see Fig. 15. The expected and measured signals have almost identical direction, gain, and the phase difference is small.

Fig. 15(c) shows that high frequent content in $\hat{\omega}_z$ is not reproduced in ω_z^{e}, even though the robot is physically capable of producing high frequent yaw motions with axis 1, which is aligned with the vertical and located approximately 3 m behind the cabin. The lack of high frequent content is then explained by the large tangential acceleration that would result from large angular accelerations of axis 1. Apparently, these cannot be compensated for by other axes. ω_x^{e} and ω_y^{e} are not affected, because these motions can be produced with axes located much closer to the head of the pilot.

Fig. 16(b) shows a detail of Fig. 15(a), from which the phase differences can be observed better. The expected roll rate appears to lag the reference by approximately 100 ms, which is in part due to a transport delay in the motion system of 48 ms. The

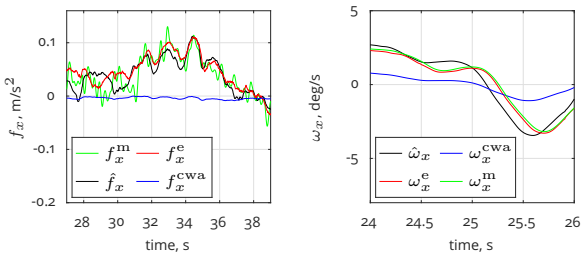

(a) Detail of Fig. 14(a). (b) Detail of Fig. 15(a).

Figure 16: Detail of example of cueing.

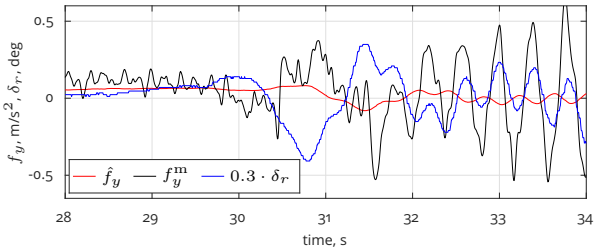

Figure 17: Example of an undamped oscillation occurring when the OM is set to "off". Control signal δ_r was scaled by a factor of 0.3 to improve visibility of other signals.

remainder is due to MPMCA attenuations, necessary to keep the system within its limits or due to the non-zero washout-term in the cost function.

7. Experiments

7.1. Experiment I: Oscillation model

A human-in-the-loop experiment was planned to assess the importance of including the OM in the MPMCA, by comparing hover performance for the OM switched on and off. The experiment was aborted after observing violent unstable oscillations in the lateral axis when the OM was switched off, i.e., if structural oscillations were *not* prevented.

Fig. 17 shows a typical oscillation, which occurred in the lateral DOF after 30 seconds of relatively stable hover. At 29.7 s, the pilot gives a slightly larger than normal control input, resulting in a small change in $\hat{f}_y$, which is, however, amplified dramatically by the actual system, see f_y^{m}. The pilot responds with a corrective δ_r command at 30.5 s resulting in $\hat{f}_y$ to change slightly in opposite direction. Again, the actual system sees a much larger change in specific force than expected. Between 29.5 and 32 s, the phase difference between the oscillations in δ_r and f_y^{m} is approximately 180 deg. Then, from 32 s onward, the phase difference is approximately zero, and the oscillations grow rapidly. At 34 s, the motion was terminated.

Similar oscillations were never observed if the OM was switched on, and thus a thorough investigation into the causality was not necessary. We believe the oscillations to be either pilot induced oscillations (PIO) resulting from delays and lag in the

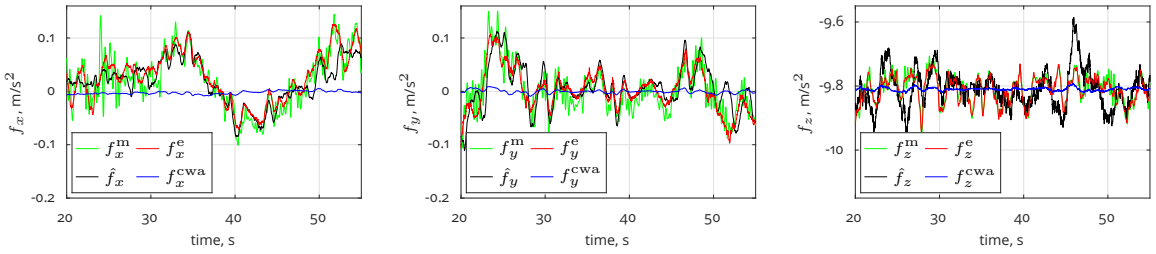

(a) Longitudinal specific force. (b) Lateral specific force. (c) Vertical specific force.

Figure 14: Example of cueing obtained by the MPMCA with PMP.

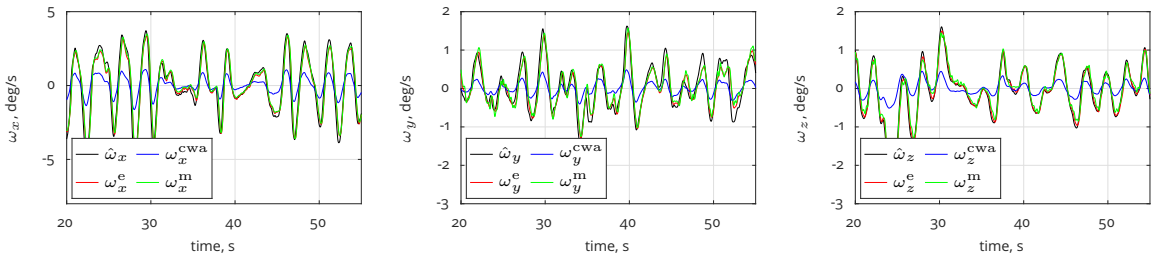

(a) Roll angular velocity. (b) Pitch angular velocity. (c) Yaw angular velocity.

Figure 15: Example of cueing obtained by the MPMCA with PMP.

entire simulation loop, aggravated by the oscillatory properties of the simulator, or caused by biodynamic feedthrough,[25] where accelerations imposed on the human arm (also a badly damped oscillatory system) result in unintended control inputs to the vehicle, that cause further accelerations and possibly unstable behavior.

7.2. Experiment II: Prediction method

7.2.1. Experiment

A computer simulation experiment was performed to compare the objective cueing performance of the EDP and PMP methods. An experienced helicopter pilot performed five trials of 60 s of hover in the simulator and his control signals were recorded. The recorded control signals were then played back to the Prediction Module, configured to use either the PMP or the EDP for 13 different values of α, and expected output was recorded for comparison.

Two objective error metrics were considered. First, the cost function output error term, evaluated over the entire 60 s:

$$J_{\boldsymbol{y}} = \sum_{j=0}^{60/t_s} ||\boldsymbol{y}^{\mathrm{e}}(j) - \hat{\boldsymbol{y}}(j)||_{W_{\boldsymbol{y}}}, \tag{27}$$

which is a measure of the total cueing quality, and second, the total normalized error for each channel separately, as defined here for f_x:

$$e_{f_x} = \sum_{j=0}^{60/t_s} \frac{\left(f_x^{\mathrm{e}}(j) - \hat{f}_x(j)\right)^2}{\hat{f}_x(j)^2}, \tag{28}$$

where t_s is the simulation time step, equal to 6 ms. The reported results are averaged over all five trials.

7.2.2. Results and discussion

Fig. 18(a) shows $J_{\boldsymbol{y}}$ as a function of α, note that results are plotted on a logarithmic scale. $J_{\boldsymbol{y}}$ is considerably lower (better) for the PMP than for the EDP method, for all values of α. At approximately $\alpha = 2.5$, the EDP method has a minimum total cost, which might indeed be a good value for actual use.

Fig. 18(b) shows the total normalized error of each channel as a function of α for the two prediction approaches. It shows that especially the angular velocities are cued much better with PMP than with EDP, for all α. Specific forces are cued better for $0.1 < \alpha < 1$ with EDP, but for these values the cueing of angular velocities is especially bad.

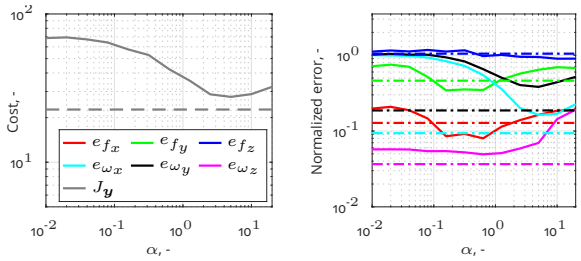

(a) Total cost. (b) Normalized error.

Figure 18: Total cost and total normalized error as a function of α. Solid lines correspond to EDP, dashed lines to PMP. Smaller values are better.

Future human-in-the-loop experiments should reveal whether the clear differences in these objective metrics are indeed indicative of the cueing quality perceived by humans. The results suggest, however, that model-free methods such as the EDP might provide acceptable cueing performance if their parameters are selected properly. This selection process will not be trivial, as α apparently also affects the trade-off between the different inertial signals. That is, a particular α might work well for a certain set of cost function weights, but not for another, complicating the tuning process.

7.3. Experiment III: Comparison to Classic Washout Algorithm

7.3.1. Experiment

A human-in-the-loop helicopter hover experiment was conducted to evaluate the functionality of the MPMCA for a variety of pilots, and to determine whether pilots achieve a comparable hover performance level as that observed with the CWA that we used in previous studies.[1,8] Based on the results of Experiment II, we selected the PMP method for use with the MPMCA. See Appendix A for a detailed description of the CWA.

Subjects were instructed to perform a helicopter hover task for 60 s and minimize the norm of the helicopter velocity vector. The first five seconds were excluded, to limit the effect of starting transients. The score, shown to the subject after each trial, represented the mean velocity vector norm:

$$D = \frac{1}{55} \sum_{j=5/t_s}^{60/t_s} t_s \sqrt{u(j)^2 + v(j)^2 + w(j)^2}. \tag{29}$$

This error metric was selected, because the limited FOV of the visual made it hard to perceive the absolute location in space, especially in the longitudinal direction. Thus, pilots did not attempt to move back to the intended hover position after drifting

forward. A position error-based performance metric would thus not be reflective of the stability of the hover: a slight drift at the start of a trial followed by a perfectly stable hover would result in a very high score. The mean velocity vector norm reflects hover performance better.

Four subjects performed the experiment: two pilots with private pilot license, with 100 and 140 flight hours on the Robinson R22 and R44, respectively, and two non-pilots with approximately 20 hours of simulator flight hours on the Robinson R44 model used in this experiment. All subjects were male, the average age was 29.5 years.

Before starting the experiment, subjects were asked to perform as many training trials without physical motion feedback as necessary, to reach a stable level of performance. On average, subjects performed 15 training trials. For each motion condition, subjects also performed as many trials as necessary to obtain a stable level of performance, after which five repetitions were collected as the measurement data.

7.3.2. Results

All subjects were able to maintain stable control of the helicopter during all trials of all conditions. The unstable oscillations, as reported in Section 7.1, were not observed. Furthermore, no trials had to be terminated due to MPMCA related problems. As such, we consider the method sufficiently robust for further experimental studies.

All subjects reported that during the MPMCA trials, they were able to perceive physical motion that "makes sense" and was "smooth". They furthermore reported that they "were actively using the motion cues", but this cannot be confirmed with objective metrics from the measured data. The CWA motion was described as "very hard to perceive" and "rough and bumpy". The latter is most likely due to the Cartesian controller attempting to avoid axes limits and the uncompensated oscillatory dynamics of the CMS. For all conditions, subjects reported it was "hard to prevent drifting".

Fig. 19 shows the obtained scores, averaged over the five measurement trials for each subject separately, and averaged over all subjects. The limited number of participants does not allow for a rigorous statistical analysis. We nevertheless observe that, 1) all participants obtained similar scores for both conditions, and 2) scores averaged over all participants are highly similar between the two MCAs.

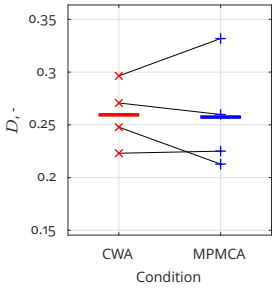

Figure 19: Mean velocity vector norm. Connected markers indicate results of individual subjects, solid lines indicate results averaged over all subjects.

7.3.3. Discussion

First, it is important to stress that a thorough evaluation of MPMCA versus CWA motion feedback is beyond the scope of this experiment. Instead, the experiment successfully showed that the MPMCA does not result in *considerably worse* hover performance than our CWA implementation. The CWA implementation cannot be improved further, given the limited Cartesian motion capabilities required by the CWA. As such, improving the MPMCA is clearly a more promising way forward.

8. Discussion

This paper presented results from the first human-in-the-loop helicopter hover experiment on a serial robot-based simulator with an MPMCA. Three experiments were presented, showing encouraging results. Still, many improvements are to be made and further experimental studies are necessary to determine whether pilots can make effective use of MPMCA motion cues. Here, we discuss the most important points for improvement.

First, we believe it to be worthwhile to investigate hybrid prediction methods that consist of simple linear filters whose form and parametrization is guided by the pilot model approach. Such methods would not require complex and computationally heavy prediction simulation schemes, but might still provide acceptable prediction performance.

The model-based approach should, however, be the first choice if the cueing performance is to be maximized. The presented pilot model-based prediction method can be improved considerably in many different areas. The method is sensitive to noise and rapidly changing control inputs, which cause the prediction to change rapidly as well. State estimation of the pilot model, based on measured inputs and control signals, might resolve this problem. The form and parametrization of the pilot model should be based on system identification

analyses with the actual helicopter dynamics, instead of creative extrapolations of experimental results with similar dynamics. Once a reliable model is obtained that works for most pilots, personalized models can be identified from or during the human-in-the-loop simulation.

Finally, improvements to the MPMCA can be made, independent of the used prediction method. The current washout position was manually selected based on insight into the kinematic properties of the robot. An optimization-based approach might reveal a better, but non-trivial, washout position. Furthermore, the currently selected output error weights were not tuned based on subjective or objective pilot feedback, which might further improve the perceived quality of the motion feedback. Note, however, that an almost perfect reproduction of a well-controlled helicopter hover should not exceed the kinematic capabilities of the robot,[10] in which case the selected output error weights would become irrelevant. That is, as the accuracy of the prediction is further improved, the need for 'tuning' the cost function weights should decrease.

9. Conclusion

This paper presented results from human-in-the-loop experiments with a novel Model Predictive Motion Cueing Algorithm (MPMCA). A central element of the method, described in detail, is a model-based prediction method, simulating a model of a human pilot in control of a helicopter. Experimental results show that the method is capable of resolving two important challenges associated with the use of serial robot-based simulators. First, the MPMCA is able to fully exploit the entire workspace of the simulator, and reproduce the inertial reference signals with high accuracy. Second, the MPMCA is able to drastically reduce unwanted oscillations in real-time, resulting from the mechanical design of the simulator, during human-in-the-loop simulations.

A. Appendix: CWA

The MCA referred to throughout this paper consists of a CWA giving position and attitude setpoits to a Cartesian Control Law (CCL) developed for the CMS. The CCL transforms setpoints in Cartesian space to setpoints for the individual axes of the serial robot.

The structure of the CWA was identical to the University of Toronto CWA[26,27]. The third-order specific force high-pass filters were identical for all DOFs:

$$H_{hp_{\boldsymbol{f}}} = \frac{s^3}{(s+0.5)^2(s+0.3)}. \tag{30}$$

The specific force low-pass filters were:

$$H_{lp_{\boldsymbol{f}}} = \frac{0.075}{(s+0.5)^2(s+0.3)}. \tag{31}$$

The angular velocity high-pass filters were:

$$H_{hp_{\boldsymbol{\omega}}} = \frac{s}{(s+0.5)}. \tag{32}$$

Based on the comments of a licensed helicopter pilot, the scaling factors for the specific forces were set to 0.1 in all DOFs. The scaling factors for angular rates were set to 0.3 in all DOFs.

For this study, we used the CCL of Ref. 7, which was later extended to use the linear rail. The CCL extends the classic kinematic inversion formulation to account for simulator joint and actuator constraints, by redefining it as a Task Priority inversion problem.[28] That is, the main task is divided into three subtasks with different priorities, in order of importance: 1) following the desired orientation, 2) following the desired position, 3) accomplish both tasks if the robot is not close to singularities.

Task Priority inversion avoids singularities and joint position limits, but does not account for velocities and accelerations limits. Hence, an additional saturation scheme is applied,[28] which prevents the *control velocity vector* from exceeding limits resulting from joint limits. Saturating the velocity vector, instead of the individual joint commands, ensures that the direction of the control vector remains unaltered, preventing off-axis distortions of the motion.

References

[1] D. Fabbroni, S. Geluardi, C. A. Gerboni, M. Olivari, L. Pollini, and H. H. Bülthoff. Quasi-transfer of helicopter training from fixed- to motion-base simulator. In *43rd European Rotorcraft Forum*, 2017.

[2] R. J. A. W. Hosman and J. C. van der Vaart. Effects of vestibular and visual motion perception on task performance. *Acta Psychologica*, 48:271–287, 1981.

[3] P. M. T. Zaal, D. M. Pool, J. de Bruin, M. Mulder, and M. M. van Paassen. Use of pitch and heave motion cues in a pitch control task. *Journal of Guidance, Control, and Dynamics*, 32(2):366–377, 2009.

[4] F. M. Nieuwenhuizen, P. M. T. Zaal, H. J. Teufel, M. Mulder, and H. H. Bülthoff. The effect of simulator motion on pilot control behaviour for agile and inert helicopter dynamics. In *35th European Rotorcraft Forum*, 2009.

[5] J. A. Schroeder. Helicopter flight simulation motion platform requirements. Technical Report NASA-TP-1999-208766, NASA, 1999.

[6] H. J. Teufel, H.-G. Nusseck, K. A. Beykirch, J. S. Butler, M. Kerger, and H. H. Bülthoff. MPI motion simulator: Development and analysis of a novel motion simulator. In *AIAA Modeling and Simulation Technologies Conference*, 2007.

[7] C. Masone, P. R. Giordano, and H. H. Bülthoff. Mechanical design and control of the new 7-DOF CyberMotion Simulator. In *IEEE Conference on Robotics and Automation*, 2011.

[8] S. Geluardi, J. Venrooij, M. Olivari, H. H. Bülthoff, and L. Pollini. Transforming civil helicopters into personal aerial vehicles: modeling, control, and validation. *Journal of Guidance, Control, and Dynamics*, 2017.

[9] A. Nesti, K. A. Beykirch, P. R. MacNeilage, M. Barnett-Cowan, and H. H. Bülthoff. The importance of stimulus noise analysis for self-motion studies. *PLOS ONE*, 9(4):1–8, 2014.

[10] M. Katliar, F. M. Drop, H. Teufel, M. Diehl, and H. H. Bülthoff. Real-time nonlinear model predictive control of a motion simulator based on a 8-DOF serial robot. In *European Control Conference*, 2018.

[11] F. M. Drop, M. Olivari, M. Katliar, and H. H. Bülthoff. Model predictive motion cueing: Online prediction and washout tuning. In *Driving Simulation Conference Europe VR*, 2018.

[12] M. Mulder, D. M. Pool, D. A. Abbink, E. R. Boer, P. M. T. Zaal, F. M. Drop, K. van der El, and M. M. van Paassen. Manual control cybernetics: state-of-the-art and current trends. *IEEE Transactions on Human-Machine Systems*, 2017.

[13] Model predictive motion cueing for a helicopter hover task on an 8-DOF serial robot simulator: Supplementary video. `https://people.tuebingen.mpg.de/fdrop/erf2018`, 2018.

[14] S. Geluardi, F. M. Nieuwenhuizen, J. Venrooij, L. Pollini, and H. H. Bülthoff. Frequency domain system identification of a robinson r44 in hover. *Journal of the American Helicopter Society*, 63(1), 2018.

[15] G. D. Padfield. *Helicopter flight dynamics : the theory and application of flying qualities and simulation modeling*. AIAA, second edition, 2007.

[16] J. Venrooij. *Measuring, modeling and mitigating biodynamic feedthrough*. PhD thesis, Delft University of Technology, 2014.

[17] R. Pintelon and J. Schoukens. *System identification: a frequency domain approach*. Wiley-IEEE Press, second edition, 2012.

[18] D. T. McRuer, D. Graham, E. S. Krendel, and W. J. Reisener. Human pilot dynamics in compensatory systems, theory models and experiments with controlled element and forcing function variations. Technical Report AFFDL-TR-65-15, 1965.

[19] M. B. Tischler and R. K. Remple. *Aircraft and rotorcraft system identification engineering methods with flight test examples*. AIAA, second edition, 2012.

[20] F. M. Drop, R. J. De Vries, M. Mulder, and H. H. Bülthoff. The predictability of a target signal affects manual feedforward control. In *13th IFAC Symposium on Human-Machine Systems*, 2016.

[21] F. M. Drop, D. M. Pool, H. J. Damveld, M. M. van Paassen, and M. Mulder. Identification of the feedforward component in manual control with predictable target signals. *IEEE Transactions on Cybernetics*, 43(6), 2013.

[22] M. M. van Paassen, J. C. van der Vaart, and J. A. Mulder. Model of the neuromuscular dynamics of the human pilot's arm. *Journal of Aircraft*, 41(6):1482–1490, 2004.

[23] F. M. Drop, D. M. Pool, M. M. van Paassen, M. Mulder, and H. H. Bülthoff. Effects of target signal shape and system dynamics on feedforward in manual control. *IEEE Transactions on Cybernetics*, 2018.

[24] D. M. Pool, P. M. T. Zaal, H. J. Damveld, M. M. van Paassen, J. C. van der Vaart, and M. Mulder. Modeling wide-frequency-range pilot equalization for control of aircraft pitch dynamics. *Journal of Guidance, Control, and Dynamics*, 34(5), 2011.

[25] J. Venrooij, M. Mulder, D. A. Abbink, M. M. van Paassen, F. C. T. van der Helm, H. H. Bülthoff, and M. Mulder. A new view on biodynamic feedthrough analysis: Unifying the effects on forces and positions. *IEEE Transactions on Cybernetics*, 43(1):129–142, 2013.

[26] L. D. Reid and M. A. Nahon. Flight simulation motion-base drive algorithms. Part 1: Developing and testing the equations. Technical Report UTIAS 296, University of Toronto, Institute for Aerospace Studies, 1985.

[27] P. R. Grant and L. D. Reid. Motion washout filter tuning: Rules and requirements. *Journal of Aircraft*, 34(2):145–151, 1997.

[28] P. R. Giordano, C. Masone, J. Tesch, M. Breidt, L. Pollini, and H. H. Bülthoff. Novel framework for closed-loop robotic motion simulation - Part I: Inverse kinematics design. In *IEEE Conference on Robotics and Automation*, 2010.